IEEE Access
Multidisciplinary | Rapid Review | Open Access Journal

Received 3 August 2022, accepted 12 September 2022, date of publication 20 September 2022, date of current version 4 October 2022.

Digital Object Identifier 10.1109/ACCESS.2022.3208143

RESEARCH ARTICLE

Monitoring COVID-19 Patients Using Cardio-Pulmonary Stethoscope RF Technology: Computer Simulation Study Using CT Scans of Patients

MAGDY F. ISKANDER, (Life Fellow, IEEE), CHRISTOPHER LEONG, (Student Member, IEEE), PRATIKSHA SHUKLA, (Student Member, IEEE), SCOTT CLEMENS, AND ZHENGQING YUN, (Senior Member, IEEE)

Hawaii Advanced Wireless Technologies Institute, University of Hawai'i at Mānoa, Honolulu, HI 96822, USA

Corresponding author: Magdy F. Iskander (magdy@hawaii.edu)

This work was supported in part by the U.S. National Science Foundation under Award IIP 1822213 and in part by the National Institutes of Health under Grant R21HL124457.

ABSTRACT In 2020, the COVID-19 pandemic claimed 3 million lives worldwide in span of a year; the death toll is still on rise as of writing of this article. Hospitals around the globe overwhelmed with COVID-19 patients faced medical resource shortages preventing them from providing services to even severe cases, leaving patients to selfcare. The identified COVID-19 patients had to observe the symptoms escalation or take imaging tests such as CT scans to determine the disease progression. While these imaging methods provide detailed accounts of damage inflicted to lungs by COVID-19, they have their own limitations and risks. In this article, we use computer simulations to examine the possibility of using the Cardio-Pulmonary Stethoscope (CPS) to continually monitor the COVID-19 afflicted lungs. Using a CT scan of a real COVID-19 patient, an infection was introduced in the lungs of an anatomically correct digital human model to be studied using simulation method. The preliminary results of simulations showed that the least detectable size of infection was an ellipsoid of 0.9 cubic cm, and the CPS was most sensitive while detecting infection in the lungs without preexisting conditions like edema. Based on the results and resolution, signal sensitivity of the CPS to COVID-19 infection is established and it can be argued that CPS could be an alternative method for continuous monitoring of COVID-19 disease.

INDEX TERMS Biomedical measurements, biomedical monitoring, mobile measurements, RF sensors.

I. INTRODUCTION

COVID-19 disease, caused by novel coronavirus SARS-CoV2, affects the epithelial cell linings of the respiratory tract and alveoli (air sacs) in the lungs. The accumulated fluids, mucus, and debris from damaged cells in the alveoli cause pneumonia resulting in hypoxia. Symptomatic patients require frequent monitoring of their situation such that supplemental oxygen can be provided on time. Aside from the observation of symptoms escalation, imaging methods like CT scan and X-ray have been employed to monitor the disease progression. Despite obtaining the accurate information on the scope of damage inflicted by COVID-19 to the lungs of infected people, these methods cannot be used for regular monitoring due to the risk of frequent radiation exposure to COVID-19 patients, risk of exposing those patients to other medical personnel, and high operational cost of the machinery. There is also the issue of resource unavailability during use and decontamination of imaging rooms after receiving a COVID-19 patient, which can take up to approximately 2 hours; these processes make the machinery a more difficult means for regular monitoring [1]. Virtual reality (VR) and artificial intelligence (AI) techniques for visualization of COVID-19 lesions have been proposed using

The associate editor coordinating the review of this manuscript and approving it for publication was Derek Abbott.

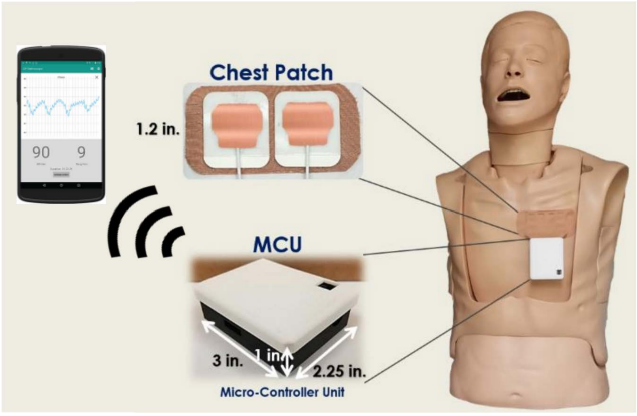

FIGURE 1. CPS system with chest patch, microcontroller unit, and mobile application.

CT scan images, however these predict the outcome of infection and do not provide a means for continuous at-home monitoring [2], [3]. Frequent use of CT and X-ray should also be avoided due to costs and radiation exposure. Furthermore, caution must be exercised when using advanced computational and optimization algorithms, such as Artificial Intelligence (AI) and Machine Learning methods, as this may lead to inaccurate assessments [4].

To achieve this objective, we propose to use the Cardiopulmonary Stethoscope (CPS), a breakthrough medical diagnostic device developed and patented on 2016 [5] and on 2020 and 2022 [6], [7] by Hawaii Advanced Wireless Technologies Institute (HAWTI). It is a pair of sensors each of which is about 34mm by 32mm at 3mm apart and uses RF (radio frequency) signals to measure the scattering parameters or S-parameters between them at 915 MHz. S-parameter is the measure of the magnitude and phase of the received signal by the non-radiating sensor, as a result of the scattered RF signal inside the patient body. This device has been validated through successful clinical trials on heart failure and dialysis patients to detect the changes in their lung water content, heart rate, and respiration rate [8]. The statistical analysis of the CPS's result against benchmark devices' result showed the correlations of $r = 0.912$ for heart rate and $r = 0.965$ for respiration rate [8], [9].

Fig. 1 shows the CPS sensor patch that measures the magnitude and phase of the S-parameters and a microprocessor unit (MCU) [10]. The original design of the sensors was described in a 1980 patent [11] and was later improved to increase accuracy and minimize signal sensitivity to movement in a design described in [12]. The device measures heart rate, respiration rate, and changes in lung water content from a single RF signal, using a combination of digital signal processing algorithms as described in earlier publications by our team [5], [9], [10], [13]. Like reflection coefficient (radar echo) and transmission coefficient across the thorax measurements, the measured S-parameter values are particularly attractive as through the ''Chest Patch'' arrangement [5], [8]. It is possible to improve accuracy (depending on patient) by optimizing the separation distance between the sensors. The MCU generates vital sign and lung water information based on data collected from the sensor and transmits it to the mobile app through Bluetooth.

In this article, we explore the possibilities of the CPS device's use in a novel application i.e., for monitoring COVID patients. The CPS has so far been used to detect changes in lung water content; measured S-parameters are highly sensitive to changes in lung tissue dielectric properties. Changes in S-parameters are correlated to changes in lung tissue. We present observations based on the simulation results of utilizing CPS for continually monitoring the COVID-19 infected lungs. The CPS's resolution on the size of identifiable inflammation and signal sensitivity to varying states of lung water content, inflammation property, spread, and location is obtained through full-wave simulations in Ansys® Finite Element High Frequency Structure Simulator (HFSS) [14]. Software based on the finite element method such as HFSS have been approved by the FCC for safety compliance [15]. The 3D EM simulations were done with a realistic digital Human Male model with over 300 objects such as bones, organs, and muscles with a 1-2mm accuracy [16]. The inflammations introduced in the digital human model's lung reflects the injury seen in the CT scan images of a real COVID-19 infected lung.

In Section II, we describe the simulation setup and Section III presents and discusses the results of these simulations. Finally, Section IV concludes the article with the observations and findings from simulation results.

II. MODELING AND SIMULATION METHOD

The regions of fluid-filled damaged alveoli in the lung are displayed as white opaque spots in CT scan images and are called ''ground glass opacity'' as they resemble the opacity of glass. As revealed from imaging test results, these infected spots are more prevalent in the lower region of the lung around its peripheral area [17]. Thus, the replication of COVID-19 infection into the lung of digital human model in HFSS was placed around lower peripheral area by creating an ellipsoid to resemble the injury seen in one of the real CT scan images of a COVID-19 patient's lungs [18]. Initially, a sphere of 11.45 mm radius was generated and scaled to the factors of 1.45 in the major axis, 0.85 in the minor axis, and 1.1 in the height axis to create the ellipsoid that represents the inflammation. The setup was executed for varying states of Lung Water Content (LWC) i.e. from normal with 20% LWC and edema with 40% LWC, to observe the signal sensitivity of the CPS in detecting the COVID-19 inflammation in lungs with and without preexisting lung conditions. The simulations were then performed by differing the inflammation size, varying the distance between the inflammation and the sensor, changing the electrical property of the inflammation, and duplicating the inflammation, for all three states of LWC.

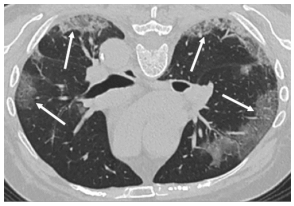

(a) CT scan image of COVID-19 affected lungs [18].

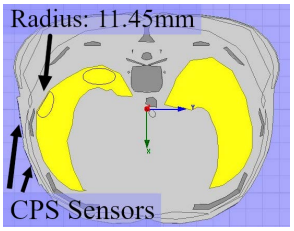

(b) HFSS model of COVID-19 infected lungs.

FIGURE 2. HFSS model and CT scan image of COVID-19 infected lungs.

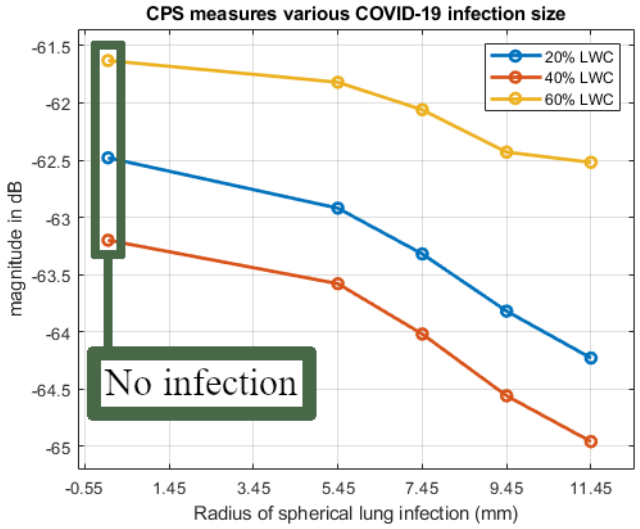

FIGURE 3. S-parameter magnitude measured by CPS for varying sizes of COVID-19 infection in different stages of lung water content.

In Fig. 2(a), we can see the reference image which is used for development of inflammation in the human model as shown in Fig. 2(b).

III. SIMULATION RESULTS AND DISCUSSION

To determine the resolution of inflammation size, the initial spherical radius of inflammation at 11.45 mm was reduced to 9.45 mm, 7.45 mm, and 5.45 mm in all cases to create the ellipsoid. By considering the electrical properties of the inflammation to be that of pure water i.e. the relative permittivity $\epsilon_r = 80$ and conductivity $\sigma = 0.01$ S/m, simulations were executed for varying states of LWC. The result of these simulations is graphically presented in Fig. 3 and Fig. 4, where the S-parameter values for different LWC at varying infection size can be seen.

In Fig. 3 and Fig. 4, values at 0 mm size of inflammation represents the lung without COVID-19 infection. As the infection is introduced to the lung, the strength of the received signal begins to deteriorate. The signal deterioration is observed to be dependent on the increment of inflammation size, and the difference between non-COVID lungs and COVID infected lungs is also seen to increase with the inflammation size increment with 5.45 mm having

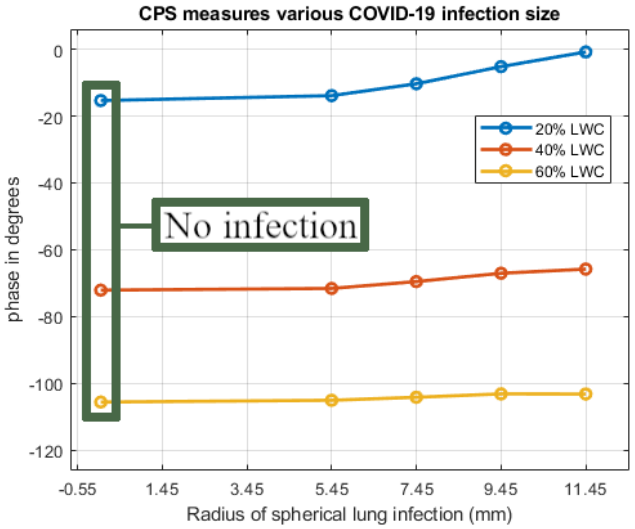

FIGURE 4. S-parameter phase measured by CPS for varying sizes of COVID-19 infection in different stages of lung water content.

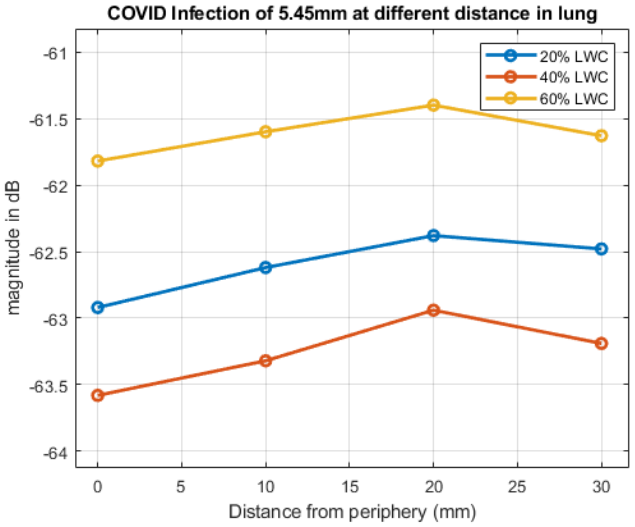

FIGURE 5. Detection of injury through S-parameter magnitude with radius of 5.45mm at various locations from the lung periphery.

the least detectable difference with non-COVID lungs. It can be inferred that the infection, once detected, can be monitored over time with the use of CPS. As more lung water is present, the narrower the margin becomes; however, it is still detectable by the CPS to monitor the state of disease spread. In addition to this, the device is more sensitive to the changes occurred for varying infection sizes on 20% LWC, and 40% LWC when compared to severe edema case i.e., 60% LWC, making it apparent that the infection growth will be easily monitored in lungs without preexisting conditions.

To determine the CPS's signal sensitivity, the least detectable size measured through these simulations i.e., 5.45 mm was moved from its location at the periphery towards the inside of the lung, away from the sensor. From its initial location, it was moved 10 mm and 20 mm inwards to

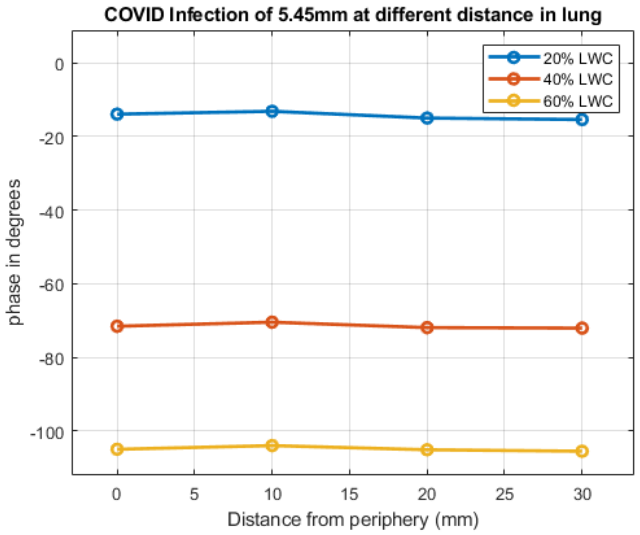

FIGURE 6. Detection of injury through S-parameter phase with radius of 5.45mm at various locations from the lung periphery.

TABLE 1. Value of fluid properties for varying stage of LWC.

LWC		Inflammation electrical property			No Infection
		Water	Blood	Mucus Membrane	
6%	dB	-58.76	-58.38	-58.45	-57.03
	Phase	35.73	34.61	33.21	25.44
20%	dB	-64.23	-63.59	-62.59	-62.48
	Phase	-0.827	-3.98	-2.67	-15.37
40%	dB	-64.96	-64.12	-64.13	-63.19
	Phase	-65.78	-66.67	-68.79	-72.07
60%	dB	-62.52	-61.93	-61.92	-61.63
	Phase	-103.14	-103.17	-104.90	-105.54

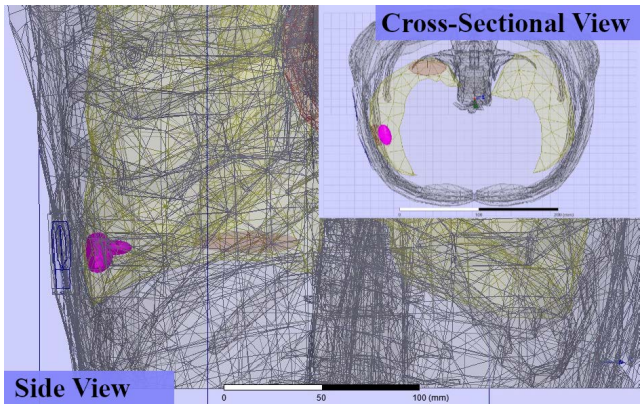

FIGURE 7. Small growth spread. Cross-sectional and side view of modeled COVID-19 injury growth (pink) in lungs (yellow). Small injury spread modeled as 9.45 mm sphere turned ellipsoid scaled at 1.45, 0.85, 0.4 in major, minor, and height axes following peripheral injury.

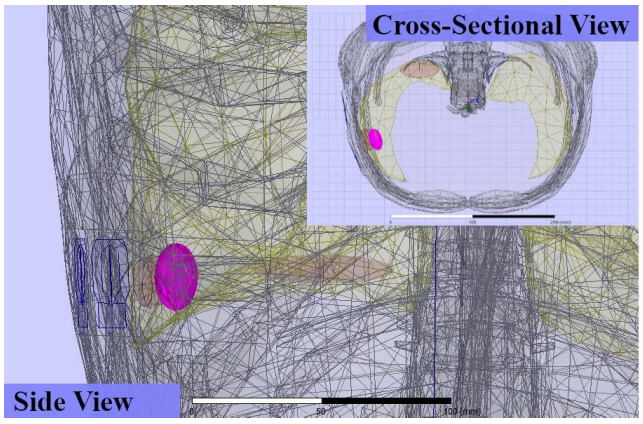

FIGURE 8. Large growth spread. Cross-sectional and side view of modeled COVID-19 injury growth (pink) in lungs (yellow). Large injury spread modeled as 9.45 mm sphere turned ellipsoid scaled at 1.45, 0.85, 1.4 in major, minor, and height axes following peripheral injury.

investigate if the CPS will be able to detect the small infection developed away from the sensors.

The results shown in Fig. 5 and Fig. 6 present the magnitude and phase respectively of S-parameter values when the injury is at varying distance from the sensors. The difference of the magnitude with non-COVID-19 case starts to decrease with the increase in distance, but the phase by comparison has little difference. However, even at the farthest distance considered in the simulation the difference measured is notable enough for its detection, except for in the case of severe edema.

In further investigation on the signal sensitivity of the CPS, simulations were performed on the inflammation of size 11.45 mm (scaled as before) by varying its electrical properties from that of pure water to blood with $\epsilon_r = 61.44$ and $\sigma = 1.55$ S/m and to mucus membrane, which has $\epsilon_r = 55$ and $\sigma = 0.948$ S/m.

Table 1 presents the result of these simulations along with the case of no infection for different states of LWC.

From the table, we can observe that when compared to no infection cases, injuries with electrical properties even slightly different than that of the lungs will be detected by CPS, as seen through the detectable change in the magnitude of the S-parameters. The higher magnitude difference with higher dielectric constant material and the lower magnitude difference with the materials with lower dielectric properties could help determine whether the infection is being consolidated with more debris and mucus or the disease is being abated.

The result of the simulation is consistent with the observation that the signal received weakens as the inflammation increases in size. It is also consistent that the difference between the infection and no infection simulations decreases as the dielectric properties of the COVID-19 inflammation and the properties of the lung are more similar.

The next set of simulations investigate the signal sensitivity of the CPS to growth of the infection via placement of a duplicated injury behind the initial infection i.e., minor spread following the initial peripheral injury. The duplicated injuries in Fig. 7 and Fig. 8 represent small and large spread

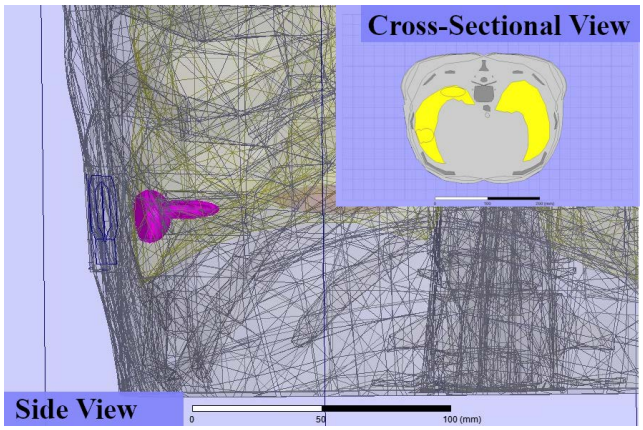

FIGURE 9. Small, wider growth spread. Cross-sectional and Side view of modeled COVID-19 injury growth (pink) in lungs (yellow). Small, wide, injury spread modeled as wide 9.45 mm sphere turned ellipsoid scaled at 1.45, 1.5, 0.4 in major, minor, and height axes following peripheral injury.

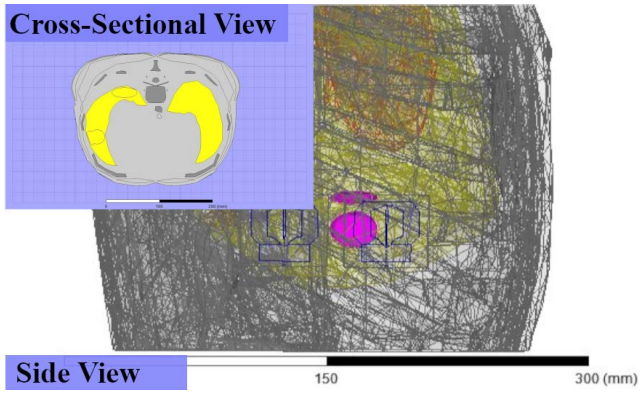

FIGURE 10. Small, wide, and elevated growth spread. Cross-sectional and Side view of modeled COVID-19 injury growth (pink) in lungs (yellow). Small and wide injury spread modeled as 9.45 mm sphere turned ellipsoid scaled at 1.45, 1.5, 0.4 in major, minor, and height axes following peripheral injury. Second grown injury placed behind peripheral injury and elevated 40 mm.

respectively. A peripheral inflammation of radius 9.45 mm was duplicated and scaled at 1.45 in the major axis, 0.85 in the minor axis, and 0.4 in the height axis to represent a thin inflammation growth 10 mm behind the peripheral injury as seen in Fig. 7. The same injury is scaled at 1.4 in the height axis to represent the large injury seen in Fig. 8.

Fig. 9 shows a wider, more circular, following injury instead of longer by scaling it at 1.5 in the minor axis instead of 0.85. Fig. 10 shows the simulation setup where the small and wider injury is elevated by 40 mm. All these cases were tested for 20%, 40%, and 60% of LWC and the results of these simulations are presented in Table 2 where they are compared against a single peripheral injury.

In Table 2, we observe that, in a normal lung i.e. lung with 20% water content, all sizes of hidden injury were detected through the decrease in signal magnitude. This holds generally true for lungs with 40% and 60% water content with the exception of small, wider, and elevated injury in case of 40% and small, wider injury in case of 60%. From this result, we can make the observation that at least for healthy lung, the CPS sensor can detect the injury that could be hidden from the direct line of sight of the sensor.

TABLE 2. Measurement value of peripheral and varying sizes of duplicate injury.

LWC		Smaller	Small-Wider	Small, wide, elevated	Large	Single Injury
20%	dB	-56.52	-56.70	-56.44	-57.67	-56.22
	Phase	-54.22	-50.34	-50.69	-86.03	-53.11
40%	dB	-57.23	-57.16	-56.70	-58.05	-56.81
	Phase	-83.33	-77.51	-79.76	-116.99	-85.66
60%	dB	-57.74	-56.63	-57.40	-58.52	-57.30
	Phase	-109.98	-80.63	-102.29	-132.19	-106.69

IV. LIMITATION OF THE STUDY

The present study is based on 2D cross sections of an average male model and emphasis is placed at location across from a suspected injured lung with the COVID-19 disease.

To determine the effectiveness of the proposed CPS RF wireless technology, additional simulations are needed and presently ongoing to quantify the effectiveness, signal sensitivity, and resolution on a variety on human models, males, females, and children, of all ages, sizes, and Body Mass Index (BMI). Preliminary results indicate that due to the chest patch-based measurements of the CPS device, the size of the human body has minimal effect on the effectiveness of the proposed COVID monitoring approach. Furthermore, in placing the CPS sensors near the suspected COVID-19 injury of the lung, it is assumed that an initial CT or X-ray scan of the patient is available or could be made. The complementary function of the CPS would be on monitoring changes in patient status including favorable response to medication and treatment, or the need for alternatives and more urgent treatments.

Some studies also suggested that water volume in lungs does not only depend on age, sex, size, and BMI of patients, but also on patient's height [19]. This clearly suggests the need for more specific 3D simulations regarding COVID inflammations and possibly additional guidelines regarding the RF sensors placement for optimized COVID monitoring. Experimental validation and conducting clinical studies [20] on COVID patients are our next steps, as we intend to follow the same approach we used in the NIH-funded clinical trials on dialysis and heart failure patients [8].

V. CONCLUSION

From the simulation results and the patterns, we observe that COVID-19 disease progression or recession could be monitored using the Cardio-Pulmonary Stethoscope (CPS). It can detect the infection on lungs up to the size as small as about 0.9 cm^3, or the volume of the smallest ellipsoid,

when the infection is around the periphery or when it is farther inside the lungs, away from sensors.

The simulation results from varying electrical properties of inflammation show that the device can indicate the presence of accumulation of substance that has different electrical property than that of lungs and can also provide information on whether the infection is getting consolidated or abated. The CPS is shown to be able to monitor inflammations consisting of blood or mucus in a severe edema patient.

In addition to this, the CPS can identify the spread of infection, even when the spread is hidden behind another infection. Since the reference value of individual patients differs based on factors such as their BMI, tissue thicknesses, etc., the CPS is best suited for monitoring and not the detection of the COVID-19 disease. The sensor should be placed centering the area of detected infection, which makes it necessary to determine where the infection resides in the lung to find the optimal location for sensor placement on the patient's body. The area of infection can be visually detected in detail through existing imaging techniques such as CT scan and X-ray. Using the CPS for monitoring COVID-19 reduces the overuse of these imaging techniques and thus reduces the risk of radiation exposure to patient and patient's exposure in medical facilities. To further improve on this work, a blind test on a few patients with preliminary set criteria is being considered for immediate action, followed by clinical trials with a broad population following a similar approach to that used in an earlier NIH-funded study on dialysis and heart failure patients [8].

REFERENCES

[1] (Mar. 2020). *CT Should Not be Used as First-Line Tool against Coronavirus, ACR Warns Following Pandemic Declaration*. [Online]. Available: www.radiologybusiness.com/topics/care-delivery/ct-scancoronavirus-chest-x-ra-radiology-covid-19

[2] A. Oulefki, S. Agaian, T. Trongtirakul, S. Benbelkacem, D. Aouam, N. Zenati-Henda, and M.-L. Abdelli, "Virtual reality visualization for computerized COVID-19 lesion segmentation and interpretation," *Biomed. Signal Process. Control*, vol. 73, Nov. 2021, Art. no. 103371.

[3] A. Qayyum, M. Mazhar, I. Razzak, and M. R. Bouadjenek, "Multi-level depth-wise context attention network with atrous mechanism for segmentation of COVID19 affected regions," *Neural Comput. Appl.*, Oct. 2021. Accessed: Sep. 25, 2022. [Online]. Available: https://link.springer.com/article/10.1007/s00521-021-06636-w

[4] M. Roberts, D. Driggs, M. Thorpe, J. Gilbey, M. Yeung, S. Ursprung, A. Aviles-Rivero, C. Etmann, C. McCague, and, "Common pitfalls and recommendations for using machine learning to detect and prognosticate for COVID-19 using chest radiographs and CT scans," *Nature Mach. Intell.*, vol. 3, pp. 199–217, Mar. 2021.

[5] M. F. Iskander, N. Celik, R. Gagarin, G. C. Huang, and D. A. Bibb, "Microwave stethoscope for measuring cardio-pulmonary vital signs and lung water content," U.S. Patent 9 526 438, Dec. 27, 2016.

[6] M. F. Iskander and R. R. Perron, "Lung water content measurement system and calibration method," U.S. Patent 10 856 806 B2, Dec. 8, 2020.

[7] M. F. Iskander and R. R. Perron, "Lung water content measurement system and calibration method," U.S. Patent 11 219 411, Jan. 11, 2022.

[8] M. F. Iskander, T. B. Seto, R. R. Perron, E. Lim, and F. Qazi, "Cardio-pulmonary stethoscope: Clinical validation with heart failure and hemodialysis patients," *IEEE Trans. Biomed. Eng.*, vol. 65, no. 5, pp. 1176–1180, Aug. 2017.

[9] N. Celik, R. Gagarin, G. C. Huang, M. F. Iskander, and B. W. Berg, "Microwave stethoscope: Development and benchmarking of a vital signs sensor using computer-controlled phantoms and human studies," *IEEE Trans. Biomed. Eng.*, vol. 61, no. 8, pp. 2341–2349, Aug. 2013.

[10] D. Bibb, R. R. G. Perron, G. C. Huang, and M. F. Iskander, "Development of a wireless monitoring system for microwave-based comprehensive vital sign measurement," *IEEE Antennas Wireless Propag. Lett.*, vol. 15, pp. 1249–1252, 2015.

[11] M. F. Iskander and C. H. Durney, "Electromagnetic energy coupler/receiver apparatus and method," U.S. Patent 4 240 445, Dec. 23, 1980.

[12] M. F. Iskander and C. H. Durney, "Microwave methods of measuring changes in lung water," *J. Microw. Power*, vol. 18, no. 3, pp. 265–275, Jan. 1983.

[13] N. Celik, R. Gagarin, H.-S. Youn, and M. F. Iskander, "A noninvasive microwave sensor and signal processing technique for continuous monitoring of vital signs," *IEEE Antennas Wireless Propag. Lett.*, vol. 10, pp. 286–289, 2011.

[14] *ANSYS HFSS. (Version 14.0)*. ANSYS. Accessed: Sep. 25, 2022. [Online]. Available: https://www.ansys.com/products/electronics/ansys-hfss

[15] *Evaluating Compliance with FCC Guidelines for Human Exposure to Radiofrequency Electromagnetic Fields*, FCC, Washington, DC, USA, Jun. 2001.

[16] M. Vogel, "Electromagnetic safety in wireless communications and bio-medical technologies," ANSYS, Canonsburg, PA, USA, Tech. Rep. MKT0000528, 2014.

[17] Fiore, Kristina. (May 29, 2020). *Hazy on Ground-Glass Opacities? Here's What They Are*. [Online]. Available: http://www.medpagetoday.com/pulmonology/generalpulmonary/86751

[18] A. Bernheim, X. Mei, M. Huang, Y. Yang, Z. A. Fayad, N. Zhang, K. Diao, B. Lin, X. Zhu, K. Li, S. Li, H. Shan, A. Jacobi, and M. Chung, "Chest CT findings in coronavirus disease-19 (COVID-19): Relationship to duration of infection," *Radiology*, vol. 295, no. 3, pp. 685–691, Feb. 2020.

[19] W. Huber, S. Mair, S. Q. Götz, J. Tschirdewahn, J. Siegel, R. M. Schmid, and B. Saugel, "Extravascular lung water and its association with weight, height, age, and gender: A study in intensive care unit patients," *Intensive Care Med.*, vol. 39, no. 1, pp. 146–150, Jan. 2013.

[20] M. Moskowitz, S. Feig, C. Cole-Beuglet, S. Fox, J. Haberman, H. Libshitz, and A. Zermeno, "Evaluation of new imaging procedures for breast cancer: Proper process," *Amer. J. Roentgenol.*, vol. 140, no. 3, pp. 591–594, Mar. 1983.

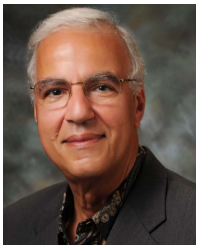

MAGDY F. ISKANDER (Life Fellow, IEEE) is currently a Professor of electrical engineering and the Director of the College of Engineering, Hawaii Advanced Wireless Technologies Institute (HAWT Institute), University of Hawai'i at Mānoa, Honolulu, Honolulu, HI, USA. Prior to joining the University of Hawaii at Mānoa, in 2002, he was the Chair Professor of electrical and computer engineering at The University of Utah, from 1977 to 2001. From 1997 to 1999, he was the Program Director at the National Science Foundation, where he formulated a "Wireless Information Technology" Initiative in the Engineering Directorate. He has authored the textbook *Electromagnetic Fields and Waves* (Prentice Hall, 1992) and (Waveland Press, 2001); the *CAEME Software Books* (Second Edition, 2012, Vol. I and II, 1991–1994); and edited four books on *Microwave Processing of Materials* (Materials Research Society, 1990–1996). He has published over 250 articles in technical journals and book chapters, 11 patents, and made numerous presentations in national and international conferences. His research is funded by the National Science Foundation, U.S. Army CERDEC, the Office of Naval Research, and several corporate sponsors. As a result of an NSF Major Research Instrumentation grant he established wireless testbed, indoor antenna range, and microwave network analysis laboratory, and an RF fabrication and characterization laboratory at the University of Hawai'i at Mānoa. His center HCAC (now HAWT Institute) had an ongoing ten-year grant, from 2005 to 2014, for partnership in the NSF Industry/University Cooperative Research Center in Telecommunications with the University of Arizona, Arizona State University, RPI, and The Ohio State University. In 2018, he established another partnership with the NSF IUCRC for Electromagnetic Compatibility with Missouri S&T University and the University of Houston. After receiving NIH grants and conducting successful clinical trials, his group established MiWa Technologies LLC, for the commercialization of their patented Cardio-Pulmonary Stethoscope Technology for monitoring vital signs and lung water measurements. His research interests include antenna design and propagation modeling for wireless communications and radar systems.

He was a member of the 1999 WTEC panel on "Wireless Information Technology-Europe and Japan," and chaired two International Technology Panels on "Asian Telecommunication Technology" sponsored by NSF/DoD, in 2001 and 2003. He was the 2002 President of IEEE Antennas and Propagation Society and a Distinguished Lecturer of IEEE AP-S, from 1994 to 1997, and a fellow of the Applied Computational Electromagnetics Society. He received many teaching excellence and research awards, including the 2012 University of Hawaii Board of Regent Medal for Excellence in Research, the 2010 Board of Regents' Medal for Teaching Excellence, the 2013 IEEE MTT-S Distinguished Educator Award, the 2010 Northrop Grumman Excellence in Teaching Award, and the 2011 Hi Chang Chai Outstanding Teaching Award. He also received the IEEE AP-S Chen-To Tai Distinguished Educator Award, in 2012, the University of Utah Distinguished Teaching Award, in 2000, the ASEE Curtis W. McGraw National Research Award, in 1985, the ASEE George Westinghouse National Education Award, in 1991, and the Richard R. Stoddard Award from the IEEE EMC Society, in 1992. Since 1992, he has been the Founding Editor of the *Computer Applications in Engineering Education* (CAE) journal (John Wiley). He edited two special issues of the IEEE TRANSACTIONS ON ANTENNAS AND PROPAGATION on "Wireless Communications Technology," in 2002 and 2006, and co-edited a special issue of *IEICE* journal, Japan, in 2004. He organized and was the general chair of nine IEEE conferences both in Utah (two) and Hawaii (seven).

CHRISTOPHER LEONG (Student Member, IEEE) received the B.S. degree in biological engineering from the University of Hawai'i at Mānoa, Honolulu, HI, USA, in 2020, where he is currently pursuing the M.S. degree in electrical engineering.

In 2020, he worked as a Research Technician at Jun Innovations. Since 2021, he has been a Research Assistant at the Hawaii Advanced Wireless Technologies Institute, University of Hawai'i at Mānoa. His current research interests include biomedical applications of electromagnetics for detection and monitoring of respiratory conditions.

PRATIKSHA SHUKLA, photograph and biography not available at the time of publication.

SCOTT CLEMENS received the B.S. and M.S. degrees in electrical engineering from the University of Hawai'i at Mānoa, Honolulu, HI, USA, in 2015 and 2018, respectively.

He has been working as a Research Assistant at the Hawaii Advanced Wireless Technologies Institute, formerly known as the Hawaii Center for Advanced Communications, since 2015. His research interests include metamaterial design and genetic programming.

ZHENGQING YUN (Senior Member, IEEE) received the Ph.D. degree in electrical engineering from Chongqing University, Chongqing, China, in 1994.

He is currently an Associate Professor with the Hawaii Advanced Wireless Technologies Institute (previously Hawaii Center for Advanced Communications, HCAC), College of Engineering, University of Hawai'i at Mānoa. His current research interests include radio propagation in complex environments, such as urban, indoor, and mountainous areas, and ocean surface and atmospheric ducts.

Dr. Yun was an Associate Editor of the IEEE TRANSACTIONS ON VEHICULAR TECHNOLOGY and the IEEE TRANSACTIONS ON ANTENNAS AND PROPAGATION. He is currently an Associate Editor of IEEE ACCESS. He has served as the Technical Program Co-Chair for the IEEE Antenna and Propagation Society International Symposium, Honolulu, in 2007, and the Technical Program Chair for the IEEE International Conference on Wireless Information Technology and Systems, Honolulu, in 2010, and Maui, HI, USA, in 2012.